Multiphoton-And SHG-Active Pyrimidine-Based Liquid Crystalline Thin Films Toward 3D Optical Data Storage

Prescillia Nicolas, Célia Minon, Stephania Abdallah, Dong Chen, Giorgia Rizzi, Yovan de Coene, Weizhen Liu, Olivier Jeannin, Thierry Verbiest, Koen Clays, et al.

ADVANCED OPTICAL MATERIALS
www.advopticalmat.de

Multiphoton-And SHG-Active Pyrimidine-Based Liquid Crystalline Thin Films Toward 3D Optical Data Storage

Prescillia Nicolas, Célia Minon, Stephania Abdallah, Dong Chen, Giorgia Rizzi, Yovan de Coene, Weizhen Liu, Olivier Jeannin, Thierry Verbiest, Koen Clays, Nathalie Bellec, Belkis Bilgin-Eran, Huriye Akdas-Kiliç, Jean-Pierre Malval, Stijn Van Cleuvenbergen,* and Franck Camerel**

An original asymmetric achiral pyrimidine core molecule, with long carbon chains on one side and a coumarin fragment on the other, is designed. This advanced molecular structure enabled the spontaneous emergence of crystalline and liquid crystalline thin films with strong 2nd harmonic generation (SHG) without any corona polishing process or tedious deposition techniques. Moreover, pin-pointed multiphoton absorption in the liquid crystalline phase effectively switches off the SHG signal locally and permanently, underlining its interest in 3D data storage. This prototypical material, which can be fully addressed by NLO processes, multiphoton writing, and SHG reading, paves the way for the development of efficient flexible materials for 3D optical data storage.

1. Introduction

The amount of numerical data generated each year continues to grow exponentially due to various factors such as the increasing digitization of industries, the proliferation of Internet-connected devices, and the rise of technologies like the Internet of Things (IoT), artificial intelligence (AI), and big data analytics. Traditional optical data storage methods have long relied on 2D surfaces to store information. However, as the volume of data generated worldwide continues to skyrocket, the need for more efficient and compact storage solutions is becoming ever more pressing. In the realm of optical data storage, 3D data storage is emerging as a revolutionary technology that is set to redefine the limits of data storage capacity, speed, and longevity. Optical 3D storage infers the ability to write and read in a pin-pointed fashion inside a material volume. One way to achieve this is to use non-linear optical (NLO) phenomena, which only occur at the focal point of a laser beam, where the energy is highest. NLO effects make it possible to selectively process voxels – volumetric pixels – whose size depends on that of the focal point in a 3D material.

For recording, the majority of the systems designed for 3D optical storage employ reversible and irreversible photochemical processes, induced by 3rd-order NLO multi-photon absorption. Typical reactions include photoisomerizations,[1] photodecompositions,[2] photo-induced dimerizations[3] and photopolymerizations.[4] Regardless of the techniques used, the general task is the same for all-optical storage devices. The reactions must create localized changes to the optical properties

P. Nicolas, C. Minon, O. Jeannin, N. Bellec, H. Akdas-Kiliç, F. Camerel
Prescillia Nicolas
Célia Minon
Olivier Jeannin
Nathalie Bellec
Huriye akdas Kiliç
Franck Camerel
Institut des Sciences Chimiques de Rennes
CNRS UMR
Université de Rennes
Rennes 35042, France
E-mail: franck.camerel@univ-rennes.fr

The ORCID identification number(s) for the author(s) of this article can be found under https://doi.org/10.1002/adom.202402083

DOI: 10.1002/adom.202402083

S. Abdallah, J.-P. Malval
Stéphanie Abdallah
Jean-Pierre Malval
Institut de Science des Matériaux de Mulhouse
CNRS-UMR 7361
Université de Haute Alsace
Mulhouse 68057, France
E-mail: jean-pierre.malval@uha.fr

D. Chen, G. Rizzi, Y. de Coene, W. Liu, T. Verbiest, K. Clays, S. Van Cleuvenbergen
Dong Chen
Giorgia Rizzi
Yovan de Coene
Weizhen Liu
Thierry Vierbest
Koen Clays
Stjin Van Cleuvenbergen
Department of Chemistry
Katholieke Universiteit Leuven
Leuven 3000, Belgium
E-mail: stijn.vancleuvenbergen@kuleuven.be

of a material, so that can later be detected and resolved. Photoisomerization which relies on the interconversion between 2 chemically stable isomer forms by photochemical reactions can be used for rewritable optical memory. Three classes of molecules (spirobenzopyran,[5] diarylethene,[6] azobenzene[7] and their derivatives) are found to be promising for this purpose. Particularly, diarylethene derivatives with heterocyclic rings exhibit no thermochromicity and have closed-ring forms that are stable for several months without showing any significant fatigue, even after 10^4 ring-opening/closing reaction cycles.[6a] Fluorescent photochromic systems have attracted particular interest because the photophysical processes are fast, efficient, and reversible.[1,6,8] However, it has been challenging to create fluorescent photochromic materials that combine high stability, high fluorescence quantum yield, and large 2-photon absorption (TPA) cross-section. Another major issue in photochromatic memory is that isomers are stable in respective single-phase bulk forms, but the bits embedded in the matrix with opposite isomer status, are liable to relax, losing contrast. Further work on material stability is apparently needed. Photodimerization can also be used to develop reversible 3D data storage media. Some small organic molecules, such as coumarin,[9] pyrimidine,[10] or anthracene[11] can undergo dimerization under multi-photon absorption and have been used for data storage in solid and polymer films. Contrary to photopolymerization and photodecomposition, the generated photodimer can be dissociated either photochemically (by UV irradiation) or thermally, offering reversibility. For example, anthracene molecules that are confined into metal-organic frameworks undergo photodimerization, which leads to reversible yellow-to-purple photoswitching of the fluorescence emission. The photoswitching behavior was used to fabricate photo patternable and erasable surfaces that, in combination with data encryption and decryption, hold promise in product authentication and secure communication applications.[12]

Amongst the optical signals that can be used for the readout, second harmonic generation (SHG) is particularly interesting since it allows high 3D resolution and rapid data acquisition using laser scanning. SHG has been obtained from corona-poled samples of poly(methyl methacrylate) polymers bearing pendant push-pull azo moieties. Two-photon absorption is employed for grayscale encoding of second harmonic signals on corona-poled thin films, thus pointing out the possibility of employing these new materials for optical data storage applications. The optical data storage has been achieved through successive isomerization cycles induced through two-photon absorption processes.[13]

More recently, it has been demonstrated that information can be stored in coumarin-based copolymer corona-poled thin films by using photo-induced dimerization.[14] In fact, the dimerization of coumarin moieties resulted in an efficient local modification of the SHG signal, which was, in turn, used to store the data. The coumarin unit undergoes a reversible photoinduced cyclodimerization by irradiation at $300 < \lambda < 400$ nm that leads to stable cyclobutane-based dimers, whereas the reverse photocleavage reaction occurs at shorter wavelengths ($\lambda < 280$ nm). However, most of these techniques based on the SHG reading are achieved in polymeric films by using the corona-poling process, in which a strong electric field is applied to align dipolar organic chromophores inside a polymer matrix near its glass transition temperature (Tg).[15] Unfortunately, after cooling, most of these corona-poled SHG-active polymeric materials lack long-term stability and reproducibility of the preparation process, while the strong electric fields used during the corona-poling process can lead to degradation.

Recently, we have demonstrated that the proper functionalization of octupolar bipyrimidine core allows the generation of chiral and flexible organic liquid crystalline thin films displaying strong SHG, competitive to inorganic crystalline materials as KH_2PO_4 (KDP), but without any corona-poling process or tedious deposition technique.[16] Here, chiral carbon chains have been grafted at the periphery of the bipyrimidine NLO-phore to provide a non-centrosymmetric molecular organization inside the thin films. We have further confirmed that the judicious functionalization of 3D organic octupoles with smaller chiral chains allows the emergence of multifunctional liquid crystalline or crystalline chromophores. These can also easily be processed into large, flexible, thin, and self-oriented films that present SHG responses without the need for corona-poling or tedious deposition techniques.[17]

Thus, it can now be anticipated that the introduction of a TPA dimerizable moiety on this class of mesogens could allow the isolation of SHG-active liquid crystalline thin films which can be used in 3D optical data storage without the use of a corona-poling process. As a proof of concept, we have designed a novel, highly asymmetric pyrimidine derivative, **PMC-3,4,5-C16** (PMC stands for Pyrimidine-Mono-Coumarin). This compound bears a coumarin moiety on one side and a promesogenic moiety on the other (**Scheme 1**), which is simpler to synthesize than a monosubstituted octupolar molecule. In contrast to our previous research, symmetry breaking is generated here by a desymmetrization of a molecule of C_{2v} symmetry and not by the introduction of chiral carbon chains. The recording upon multiphoton dimerization of the coumarin moieties should result in a pin-pointed modulation of the SHG signal generated by the non-centrosymmetric organization of the chromophores inside the liquid crystalline matrix.

2. Results and Discussion

PMC-3,4,5-C16 has been synthesized in 3 steps. Compound **1** was obtained as a white powder by a Knoevenagel condensation[18] between the commercial *4,6-dimethylpyrimidine* and *4-bromobenzaldehyde* in strong basic condition (NaOH, 5 M). Compound **4** was freshly prepared according to a literature procedure.[19] Its synthetic route begins with the substitution of the hydroxyl group on *7-hydroxycoumarin* by a better triflate leaving group (-OTf) to perform Sonogashira coupling with *TMS-acetylene* and give alkyne-coumarin **4** after deprotection of the TMS function. Next, compound **4** was grafted onto one bromide position of compound **1** via Sonogashira copper-free cross-coupling (SCFCC). Product **5** precipitates, making it easy to isolate by filtration. However, its poor solubility

B. Bilgin-Eran, H. Akdas-Kiliç
Huriye Akdas-Kiliç
Belkis Bilgin-Eran
Department of Chemistry
Yildiz Technical University
Istanbul 34220, Turkey

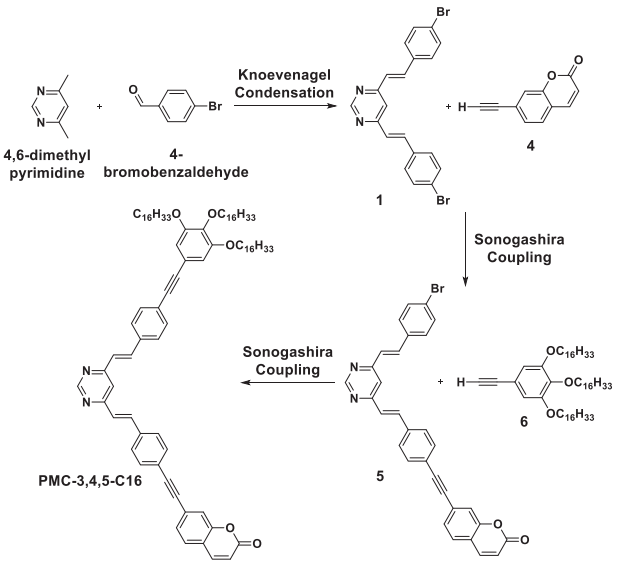

Scheme 1. Synthetic pathway used to obtain the targeted **PMC-3,4,5-C16** compound.

prevented a correct characterization of this product, which was used in the next step without purification. *5-ethynyl-1,2,3-tri(hexadecyloxy)benzene*, **6**, was synthesized according to a literature procedure,[20] and its grafting by SCFCC on the remaining bromide position of compound **5** allowed to obtain the targeted **PMC-3,4,5-C16** compound as a yellow powder in good yield (55%). ^{1}H and ^{13}C NMR studies and Elemental analysis confirm the formation and the purity of the targeted compound (see SI for all experimental details, Figures S1–S10, Supporting Information).

The liquid crystalline properties of **PMC-3,4,5-C16** were fully investigated by Polarized Optical Microscopy (POM), Differential Scanning Caalorimetry (DSC), and Small Angle X-ray Scattering (SAXS). Between crossed polarizers, at room temperature, this compound appears as a yellow and birefringent solid (Figure S11a, Supporting Information). Upon heating, it begins to melt into a fluid and birefringent material ≈125 °C, highlighting the formation of a liquid crystalline phase. With further heating, it starts to melt into an isotropic liquid at 147 °C (Figure S11b, Supporting Information). Cooling from the isotropic state, an uncharacteristic fluid texture with ill-defined broken fan shapes readily develops below 135 °C (**Figure 1a**; Figures S11c, Supporting Information). Upon further cooling, a texture change is observed at 110 °C and the compound becomes difficult to deform under pressure, indicating a crystallization of the compound at low temperatures (Figure S11d, Supporting Information). DSC traces display a highly energetic reversible thermal transition centered at 119 °C, in line with the crystal-to-mesophase transition observed by POM (Figure 1b; Figure S12, Supporting Information). The transition between the liquid crystalline state and the isotropic liquid was only detected on the cooling DSC traces

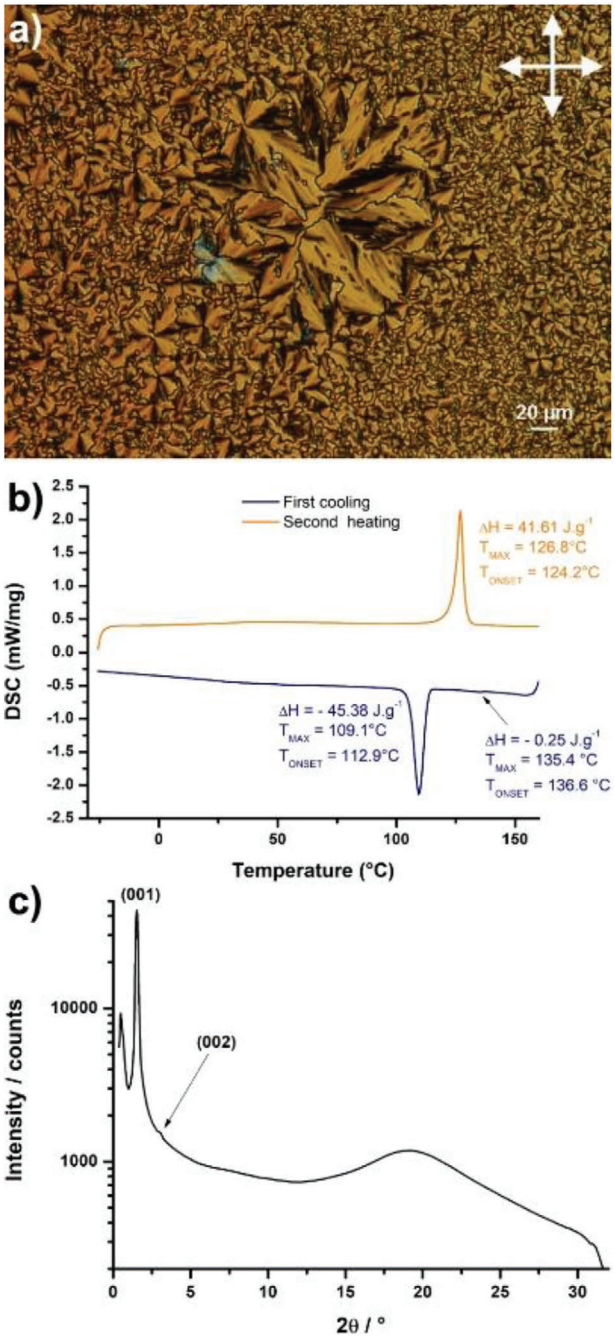

Figure 1. a) Optical photomicrograph of the **PMC-3,4,5-C16** compound obtained with a polarizing microscope at 132 °C upon cooling from the isotropic state (crossed-polarizers symbolized by the white cross in the corner of the picture); b) DSC traces of **PMC-3,4,5-C16** (scan rate: 10 °C min^{-1}), 2nd cooling and 1st heating between −25 and 160 °C; c) SAXS patterns of **PMC-3,4,5-C16** recorded at 140 °C upon heating (c).

with an onset at 136 °C. Temperature-dependent SAXS measurements were performed to confirm the emergence of a liquid crystalline phase (Figure S13, Supporting Information). At low temperatures, the SAXS patterns are characteristic of a crystalline phase with several sharp diffractions over the whole 2θ range.

Interestingly, the sharp diffraction peaks in the small-angle region correspond to the (00l) reflections from a lamellar phase (Figure S13, Supporting Information), showing that the compound organizes into lamellae. The diffraction patterns recorded between 140 and 120 °C when cooling and 125 and 150 °C when heating display only 2 sharp diffraction peaks in the small angles region in a ratio 1:2. Regarding the organization observed in the crystalline phase, these peaks can be considered as the 2 first reflections of a lamellar phase (Figure 1c; Figure S14, Supporting Information). The broad halo centered at 19° in 2θ indicates that the carbon chains are in a molten state and confirms the liquid nature of the organized phase in these temperature ranges. These diffraction patterns are characteristic of a liquid crystalline phase and show that the compound organizes into a smectic mesophase. Since the optical texture is deprived of the presence of homeotropic domains, the molecules are surely tilted inside the smectic layers, suggesting the formation of a smectic C phase. Above 150 °C, the SAXS patterns only display one low-intensity broad halo in the small angle region as expected for an isotropic phase. In the liquid crystalline phase at 140 °C, the lamellar period is 57.6 Å. Geometry optimization of the molecule by DFT calculations shows that the molecule is strongly bent around the central pyrimidine core. The length of the molecule in its fully extended configuration is ≈51.8 Å (FigureS15, Supporting Information) and corresponds roughly to the lamellar period, indicating that the molecules are likely stacked in head-to-tail fashion inside a monolayer (see model in Figure S16, Supporting Information). Due to the bent nature of the molecule and the strong SHG activity of the mesophase (vide infra), it cannot be excluded that the molecules are organized into a cooperative non-symmetric stacked or chiral B2 phase.[21] Additional investigations need to be performed to better elucidate the molecular packing inside the smectic C mesophase.

The photophysical properties of the **PMC-3,4,5-C16** compound were first investigated in solution. **Figure 2** displays the one- (1PA) and two-photon (2PA) absorption spectra of the dye as well as their respective fluorescence spectrum in solution in THF. **Table 1** gathers the related spectroscopic data. The low energy side of the 1PA spectrum of **PMC-3,4,5-C16** is dominated by a single and intensive band located in the 320–430 nm range (Figure 2a; Figure S17, Supporting Information). This unstructured band also displays a shoulder on its blue edge suggesting the presence of several S_0-S_n transitions. The excitation anisotropy spectrum of the dye and TD-DFT calculations both corroborate the presence of multiple electronic transitions within this longest wavelength absorption band. As shown in Figure S17 and Table S3 (Supporting Information), the theoretical absorption spectrum of **PMC-3,4,5-C16** reasonably agrees with its experimental one and confirms the presence of 4 S_0-S_n transitions positioned in the 345–450 nm range. The lowest energy transition (i.e., S_0-S_1) is strongly allowed (f>2) and presents a $\pi\pi$*-type

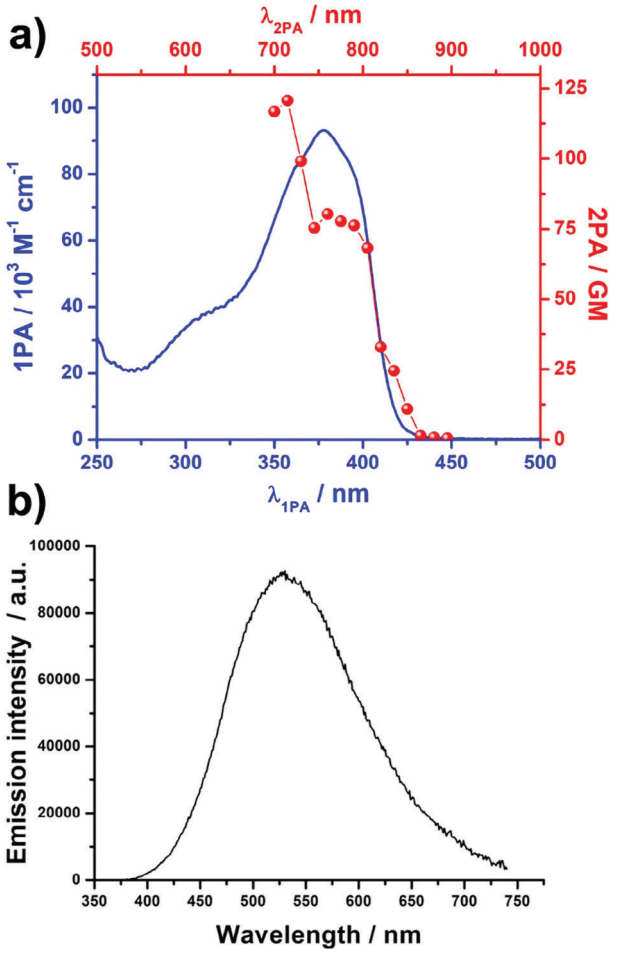

Figure 2. a) 1PA (blue line) and 2PA (red circles) spectra of **PMC-3,4,5-C16** compound in THF; b) fluorescence spectra of **PMC-3,4,5-C16** compound in THF.

character implying a long-range electronic delocalization from the trialkoxy substituted stilbenyl branch to the coumarin one (see **Figure 3**). This lowest energy transition should correspond to an intramolecular charge transfer transition (ICT) with a typical planar geometry that presumably authorizes such a long-range electronic conjugation. Moreover, the average value for the anisotropy of the $S_0 \rightarrow {}^1$ICT transition is ≈0.34 ± 0.01. This high value indicates that the transition moment at the ICT state is roughly collinear to that of the ground state which corroborates the weak electronic and/or geometric relaxation of the emitting ICT state. Note that the S_0-S_2 transition which is positioned ≈390 nm also displays a $\pi\pi$*-type character but is mainly localized on a single π-conjugated branch of the dye. Such distinctive

Table 1. One- and Two-Photon Spectroscopic data of **PMC-3,4,5-C16** compound in THF.

	ϵ_{abs} [M^{-1} cm^{-1}]	λ_{1P} [nm]	λ_{fluo} [nm]	E_{00} [a] [eV]	Φ_{fluo}	τ_{fluo} [b] [ns]	k_r [c] [10^9 s^{-1}]	k_{nr} [c] [10^9 s^{-1}]	$\frac{k_{nr}}{k_r}$	λ_{2P} [nm]	δ_{2P} [d] [GM]
PMC-3,4,5-C16	93270	378	532	2.81	0.39	1.48	0.26	0.41	1.58	715	121

[a] $E_{00} \approx ½\, hc(\nu_{abs} + \nu_{fluo})$; [b] Average fluorescence lifetime from a bi-exponential fit; [c] $k_r = \Phi_{fluo}/\tau_{fluo}$ and $k_{nr} = (1\text{-}\Phi_{fluo})/\tau_{fluo}$; [d] The uncertainty in δ is ± 15%.

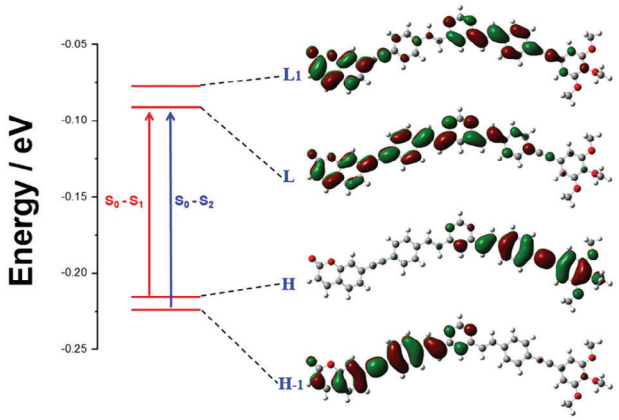

Figure 3. Frontier molecular orbitals (MO) diagrams of **PMC-3,4,5-C16** with its 2 lowest energy S_0-S_1 and S_0-S_2 transitions.

electronic configurations between S_0-S_1 and S_0-S_2 transitions are also in line with the decrease of the excitation anisotropy between 425 and 385 nm which indicates the presence of electronic transitions with different polarizations. Interestingly, this anisotropy decreases further going into the high energy region and reaches a plateau below 345 nm. Such a change in anisotropy clearly echoes the occurrence of additional S_0-S_n transitions, presumably the S_0-S_3 and S_0-S_4 ones, which are also well predicted by the theoretical calculations. The 2PA spectrum has been plotted against half the excitation wavelength in order to have a direct comparison with the 1PA one (see Figure 2). A maximum two-photon absorption cross-section of ≈120 GM has been measured for this compound in the 680–900 nm range. According to our spectral resolution, 2 distinctive bands positioned in the same spectral range as the longest wavelength 1PA band can be observed which corroborates our previous analysis. However, it should be noted that the maximum 2PA band does not match the 1PA one. Such an unexpected effect for a π-conjugated dye with an asymmetrical geometry is paradoxically similar to that observed for centrosymmetric V-shaped pyrimidine systems[22] for which the lowest energy transition is theoretically 2-photon forbidden. This compound is highly luminescent with a quantum of 0.39 in THF. The corresponding fluorescence band is located in the 425—680 nm range with a maximum of 532 nm. Hyper-Rayleigh Scattering (HRS) was employed to determine the second-order nonlinear optical properties of **PMC-3,4,5-C16** (Table 1). HRS experiments were performed in chloroform at 1300 nm. This wavelength was selected to minimize the multiphoton fluorescence (MPF) contribution to the HRS signal. Nonetheless, the overwhelming MPF made it impossible to observe any second-order nonlinear hyper-Rayleigh scattering. This is most likely due to the molecular single pyrimidine design, which lacks the octopolar D2, quasi-tetrahedral symmetry that was used in the previous designs.[16,18] It also misses a strong acceptor-donor substitution pattern for the classical dipolar design. Congruent with the proposed HOMO and LUMO (Figure 3), the alkoxygroups are the electron-donating groups, but alkoxy substituents are weaker than dialkylamino ones. The coumarin group is also a not very efficient electron acceptor. The fact that efficient SHG was detected from the liquid crystal thin film mesophase points to the importance of the cooperative non-centrosymmetric stacking in that phase (see above).

A thin film of **PMC-3,4,5-C16** was then prepared between 2 glass plates (thickness ≈20 µm, Figure S18, Supporting Information) and heated to the liquid crystal phase (≈130 °C) to obtain a homogenous birefringent texture between crossed polarizers. The film was irradiated with a UV source linked to the microscope (340–380 nm) using a 50x objective (Nikon, CFI Plan). This UV wavelength range was chosen because it usually induces photodimerization of coumarin fragments and corresponds to the absorption range of the molecule. The temperature was maintained at 130 °C during the entire irradiation. After 10 s of exposure and switching to a 5x objective (Nikon, CFI Plan), a black dot clearly appeared on the birefringent films (**Figure 4a**), showing that the area where the liquid crystalline phase was irradiated became amorphous. This black spot was found to be stable upon heating into the isotropic state at 150 °C, as upon cooling it reappeared in the middle of the birefringent liquid crystalline phase. The UV printing is stable after several heating-cooling cycles and persists for several weeks at room temperature after cooling into the crystalline phase. This process was repeated to obtain 4 different irradiation areas (Figure S19, Supporting Information). Such irradiation experiments have also been attempted at room temperature in the crystalline phase, but the writing process is much less efficient and requires several minutes of irradiation to observe a slight extinction of the birefringent phase. The switching of the optical properties under UV irradiation is thus facilitated in the fluid-liquid crystalline phase. To establish their potential for application in NLO data storage devices, good-quality thin films with a large homogeneous surface, printed with black dots as described above, were measured by spectral SHG at 1030 nm (Figure 4b). Under the same experimental conditions, the organized birefringent phase shows a strong SHG activity whereas, in the irradiated area, it has almost vanished. In the liquid crystalline phase, the strong SHG peak at 515 nm rises above a broad (multiphoton) fluorescence background (Figure S20, Supporting Information). It should be noted that high SHG activity was achieved in the liquid crystalline phase without the introduction of chiral carbon chains, and also without the octupolar, quasi-tetrahedral symmetry, as was the case with bipyrimidine cores.[16–18] This signal is strongly attenuated in the irradiated regions by 75% (**Figure 5**). These measurements show that good SHG contrasts can be obtained between the irradiated and the non-irradiated areas and that the SHG signal, which is associated with high 3D resolution, can therefore be used for the readout of the stored information within such liquid crystalline thin films. To demonstrate that 3D writing can also be achieved, three-photon photo-printing tests (λ_{irr} = 1030 nm) in the liquid crystal phase (130 °C) with a scanning multiphoton microscope (22.5 mW input power after the 20x/0.5 Na objective) were also carried out. Considering the absorption band of the compound and the excitation wavelength used in this experiment, the three-photon absorption occurs at 343 nm, which is in the same range as the previously applied UV light. As three-photon absorption is inherently localized to the focal point of the objective, we were able to print well-defined regions with submicrometer resolution. As shown in Figure 4c, 3 well-defined squared areas of different sizes have been imprinted on the liquid crystalline thin films. As observed for direct irradiation with

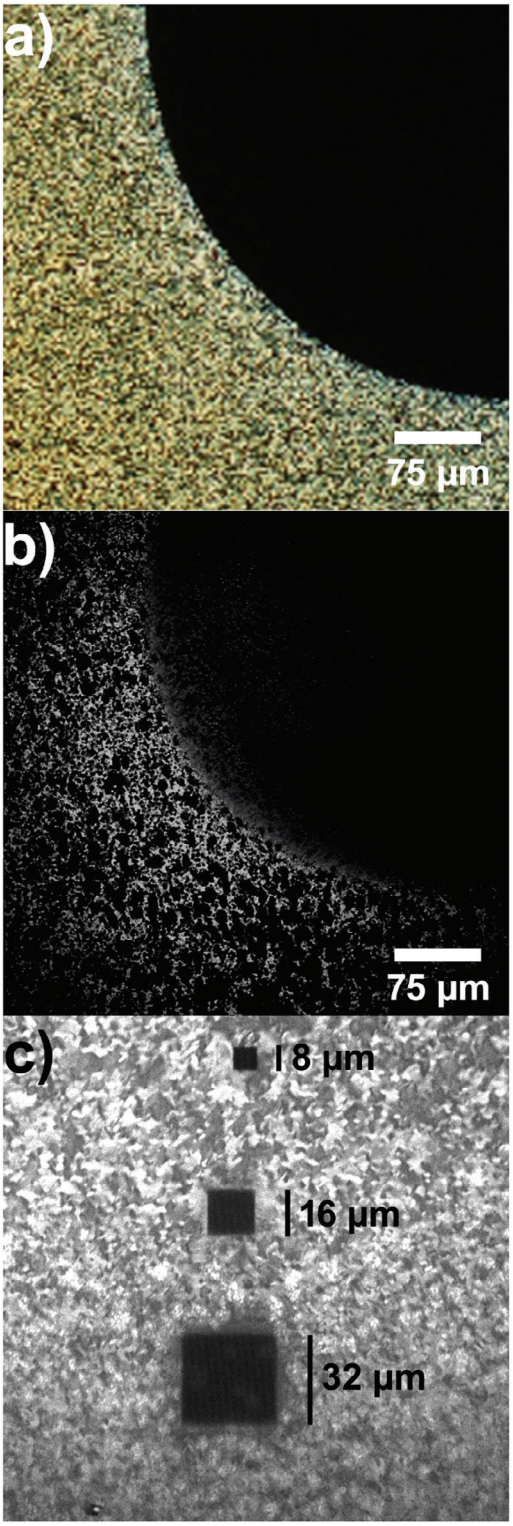

Figure 4. a) Optical photomicrograph of the **PMC-3,4,5-C16** compound obtained with a polarizing microscope at 130 °C upon cooling from the isotropic state after irradiation with the microscope UV source at 340–380 nm during 10 s (scale bar 75 µm); b) optical photomicrograph of the same area at room temperature with SHG filter (scale bar 75 µm); c) optical photomicrograph with SHG filter after irradiation with a scanning multiphoton microscope at 1030 nm at 130 °C.

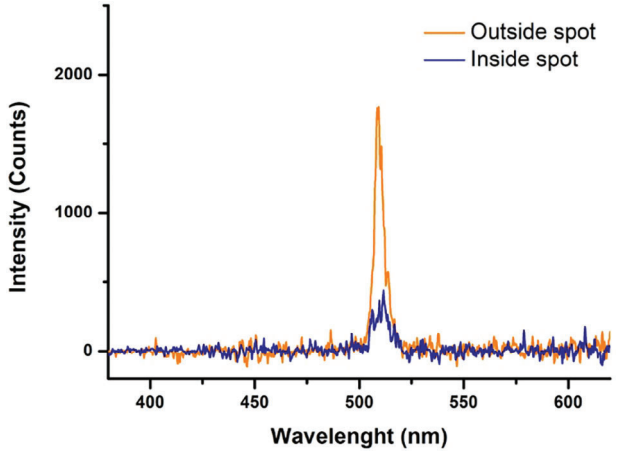

Figure 5. SHG spectra were obtained for compound **PMC-3,4,5-C16** inside (blue line) and outside (orange line) the irradiated area (black spot in Figure 5b).

UV light, three-photon irradiation resulted in a strong attenuation of the SHG activity in all the printed regions, remaining stable after cooling to room temperature. For technical reasons, having only a 1030 nm laser, three-photon absorption was used for writing, but it would be more appropriate to use two-photon absorption at 700 nm to avoid overlap with SHG reading. The loss of SHG signal in the irradiated area can be attributed to the local amorphization of the non-centrosymmetric supramolecular packing in a centrosymmetric amorphous phase induced by the photodimerization of the coumarin fragments or photoisomerization of the styryl bonds. Alternatively, photobleaching of the molecule has to be considered as well.

In order to have more insights into what is happening inside the UV-exposed area, a thin film of **PMC-3,4,5-C16** was fully irradiated at 340–380 nm with the microscope UV source until it became completely black under crossed-polarizers. The entire film was then dissolved in a deuterated solvent and ^{1}H NMR was performed. In the case of a photodimerization of the coumarin fragments, the 4 dimers resulting from the [2+2] photocycloaddition reaction should show new signals between 3 and 5 ppm.[23] Here, after UV irradiation of the film, no such ^{1}H NMR signals have been observed (Figures S21 and S22, Supporting Information). In addition, if the optical switching of the irradiated area is induced by a photodimerization of the coumarin, this process should be reversible under higher energy UV excitation at 254 nm.[1c,10,15] Several irradiation experiments performed using a UV Rayonnet at 254 nm at room temperature or in the liquid crystalline phase at 130 °C have shown that the writing process is completely irreversible and the black area remains unchanged. These experiments confirm that the change of the optical properties in the irradiated areas is not induced by the photodimerization of the coumarin fragments as initially expected. In addition, new signals appear in the aromatics region of the ^{1}H NMR spectrum of the irradiated film and the baseline is more ill-defined compared to the product before irradiation, which could be explained by the partial photodegradation of the product under irradiation. The percentage of photodegradation, evaluated by NMR, shows that almost 20% of the compound has been decomposed

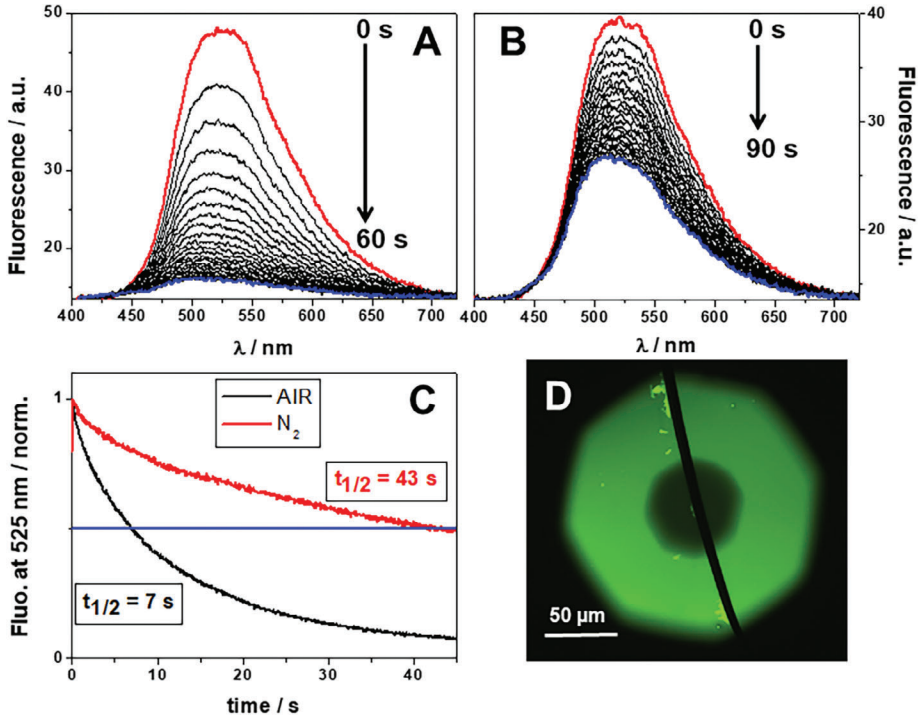

Figure 6. Evolutions of the fluorescence spectra of spin-cast films of the dye upon excitation at 365 nm: A) Under air stream. B) Under N_2 stream. C) Comparison of the time-dependent fluorescence intensity changes of **PMC-3,4,5-C16** films under air and N2 atmosphere. D) Epifluorescence image of a spin cast film of **PMC-3,4,5-C16** after 1 min excitation at 365 nm in air atmosphere. Note that the small octagonal dark area denotes the excitation zone. A scratch has been made on the spin-cast film to emphasize the luminescent contrast.

under UV irradiation. This demonstrates that only a small fraction of the molecules need to be converted to almost completely change the optical properties of the irradiated area. All these observations point to photobleaching rather than photodimerization or even photoisomerization of styryl bonds. To further confirm this hypothesis, the solid-state emission of the compound was excited both under air and under an inert atmosphere (N_2) (**Figure 6**). Under air, the luminescence signal centered at 515 nm drastically decreases under UV irradiation at 340–380 nm. The same process is also observed under nitrogen, but the kinetic of the reaction is 4 times slower than the one of the measurements performed under air. The photobleaching of the molecule can thus be explained by the generation of singlet oxygen after intersystem crossing (ISC) to a triplet state. The formation of this very reactive species will rapidly degrade the molecule in the irradiated region, changing the organization of the liquid crystal phase to an isotropic phase. The lower efficiency of the photodecomposition process under UV irradiation observed in the crystalline phase is likely attributed to lower oxygen diffusion within the thin film thickness compared to the fluid phases. Nevertheless, even if it is photobleaching instead of photodimerization, we are still able to write a stable information inside a bulk material by multiphoton absorption and to read it by high-3D resolution SHG.

3. Conclusion

To conclude, an original molecule with a highly asymmetric bent-core has been designed around a pyrimidine core with an alkynyl-styryl coumarin moiety on one side and an alkynyl-styryl hexadecyloxy moiety on the other. This molecule is capable of organizing into a noncentrosymmetric smectic C phase between 120 and 140 °C, and exhibits high SHG activity. Irradiation in the liquid crystalline phase enables rapid encoding of information by disrupting molecular organization in a non-SHG active isotropic phase after multiphoton absorption. However, the writing process is not induced by a photodimerization of the coumarin fragment as expected but by a photobleaching/photodecomposition of the molecule under laser irradiation in the presence of oxygen. The electron density delocalization through the alkynyl-styryl arm probably deactivates the photodimerization ability of coumarin fragments. Nevertheless, such active NLO thin films hold great promise for 3D optical data storage, as they enable pin-pointed multiphoton writing and pin-pointed SHG reading. Future work will now focus on decreasing the temperature range of the liquid crystalline phase around room temperature and restoring the dimerization capacity of coumarin prior to photobleaching in order to reach a fully reversible 3D data storage device.

4. Experimental Section

Full synthetic details for the preparation of **PMC-3,4,5-C16** compound and its intermediates are given in supporting information. 300 or 500 (^{1}H) and 75.5 or 126 MHz (^{13}C) NMR spectra were recorded on Bruker Avance 300 or 500 spectrometers at room temperature using residual proton solvents as internal standards. Elemental analyses were performed by the Service de Microanalyse BioCIS, Faculté de Pharmacie, Université Paris-Saclay, Orsay, France.

DSC was carried out by using a NETZSCH DSC 200 F3 instrument equipped with an intracooler. DSC traces were measured at 10 °C min^{-1} down to −25 °C.

Optical microscopy investigations were performed on a Nikon H600L polarizing microscope equipped with a Linkam "liquid crystal pro system" hostage LTS420. The microscope is equipped with a UV irradiation source (Hg Lamp, λ = 340–380 nm) which was used for the writing on the LC films. The microscope is also equipped with an Ocean Optic USB 2000+ UV-Vis-NIR spectrophotometer and a UV-2A filter cube for recording luminescence spectra under UV irradiation at 340–380 nm.

X-ray scattering experiments were performed using a XENOCS GeniX3D low convergence copper micro source (50 W) equipped with FOX3D single reflection optics and point collimation. The patterns were collected with a Mar345 Image-Plate detector (Marresearch, Norderstedt, Germany). The samples were held in Lindeman glass capillaries (1 mm diameter). The capillaries were placed inside a Linkam HFX350-Capillary X-Ray stage which allows measurements from −196 up to 350 °C with an accuracy of 0.1 °C.

The two-photon absorption (2PA) measurements were performed with femtosecond mode-locked laser pulse using a Ti: Sapphire laser (Spectra-Physics, Mai Tai: pulse duration: ≈100 fs; repetition rate: 80 MHz; wavelength range: 690–1040 nm). A relative two-photon excited fluorescence method[24] was employed to measure the two-photon absorption cross-sections, δ. The measurements of 2PA cross-sections were performed relative to reference molecules (r) such as fluorescein[25–27] in water at pH 11. The value of δ for a sample (s) is given by:

$$\delta_S = \frac{S_S \Phi_r \eta_r c_r}{S_r \Phi_S \eta_S c_S} . \delta_r \quad (1)$$

where S is the detected two-photon excited fluorescence integral area, c is the concentration of the chromophores and Φ is the fluorescence quantum yield of the chromophores. η is the collection efficiency of the experimental set-up and accounts for the wavelength dependence of the detectors and optics as well as the difference in refractive indices between the solvents in which the reference and sample compounds are dissolved. The measurements were conducted in a regime where the fluorescence signal showed a quadratic dependence on the intensity of the excitation beam, as expected for two-photon induced emission. For the calibration of the two-photon absorption spectra, the two-photon excited fluorescence signal of each compound was recorded at the same excitation wavelength as that used for standards. The laser intensity was in the range of 0.2–2 × 10^9 W cm^{-2}. The experimental error on the reported cross-section is 15%.

The absorption measurements were carried out with a Perkin Elmer Lambda 2 spectrometer. Steady-state fluorescence spectra in solution were collected from a FluoroMax-4 spectrofluorometer. Emission spectra are spectrally corrected, and fluorescence quantum yields include the correction due to solvent refractive index and were determined relative to quinine bisulfate in 0.05 molar sulfuric acid (Φ = 0.52).[28]

The fluorescence lifetimes were measured using a Nano LED emitting at 372 nm as an excitation source with a nano-led controller module, Fluorohub from IBH, operating at 1 MHz. The detection was based on an R928P-type photomultiplier from Hamamatsu with high-sensitivity photon-counting mode. The decays were fitted with the iterative reconvolution method on the basis of the Marquardt/Levenberg algorithm.[29] Such a reconvolution technique allows an overall time resolution down to 0.2 ns. The quality of the exponential fits was checked using the reduced $\chi 2$ (≤1.2).

For Hyper-Rayleigh scattering measurements, a custom-designed optical setup was used to determine the first hyperpolarizabilities of the compounds. The laser (Insight DS+, Spectra-Physics) allows for a tunable output between 680 and 1300 nm. The former delivers femtosecond (≈120 fs) pulses at an 80 MHz repetition rate. The output beam (1/e2 < 1.2 mm) has a Gaussian profile (M2 < 1.1) and is horizontally polarized (the plane of the optical table). A combination of an achromatic half-wave plate and a Glan-Laser polarizer allows for control of the output power in accordance with Malus's law. The polarizer is placed in such a way that the extraordinary ray is vertically polarized. The average power which is sent into the sample typically ranges from 500 to 1000 mW. The beam is routed to the input lens (aspheric, f = 8.00 mm) by a series of mirrors. A long pass filter with a cut-off at 690 nm is used to prevent any higher harmonic generation from the laser or the optics from entering the sample. The quartz cuvette (10 × 4 mm) is placed in a custom translation mount which allows to definition of the path length of the focal point relative to the side walls. Light is collected at 90° by an achromatic, aspheric condenser lens (f = 30 mm). The collimated beam passes a series of 3 large broadband dielectric elliptical mirrors to rotate the image 90°. The latter ensures maximal resolution of the spectrograph (vertically oriented slit). The collimated beam is focused on the spectrograph (IS/SM 500, Bruker) with a plano-convex lens, matching the focal length of the spectrograph (f = 200 mm, f/8). A blocking edge filter (FF01-720/SP-25, Semrock) ensures high optical density in the laser excitation range. One of 2 gratings (50 grooves/mm, 600 nm blaze or 150 grooves/mm, 500 nm blaze) were used, depending on the desired resolution, diffraction range, and spectral profile of multiphoton emission spectra. An EMCCD camera (Ixon Ultra 897, Andor Solis) was used to image the spectra.

Thin film thickness was measured using a Bruker DektakXT stylus profilometer.

For SHG imaging, the sample was illuminated wide field under normal incidence with femtosecond pulsed infrared (IR) laser light at 1030 nm (Pharos, Light Conversion). The intensity and polarization of the incident IR light is varied by a combination of a zero-order half-wave plate for 1030 nm mounted in a computer-controlled rotation stage (Thorlabs, PRM-Z8) and a Glan-Taylor polarizer selecting for S-polarized light. The sample is irradiated by a long focal length lens (f = 5 cm) which is focused above the sample so that the incident fundamental light can be considered to a good approximation as a collimated beam and electric field components along the propagation direction (Z) can be neglected. Behind the sample, a 20x objective (Nikon, CFI Plan Fluor 20X CH) collects the light. In the infinity path an IR filter rejects the laser light and a filter wheel selects the transmitted wavelength for SHG (Bandpass, 515 nm, Edmund Optics #65-153), MPF (Longpass, Cut-off wavelength 525 nm, Edmund Optics #84-744) or Bright field (no filter). A 20 cm tube lens (Mitutoyo) then images the light onto the slit of an imaging spectrometer (Andor, Kymera 328i), coupled to an I-CCD camera (Andor, iStar 340). By switching between a mirror and a grating (150 l mm^{-1} groove density; blaze = 500 nm), the spectrometer can be used for imaging and spectroscopy respectively. The latter option requires closing the slit of the spectrometer to ensure adequate spectral resolution. For the bright field imaging, an LED source mounted above the sample was used. This LED source could be polarization selected by a broadband polarizing sheet, positioned perpendicular to a rotatable broadband polarizer in the detection path. In this manner, polarized optical microscopy images could be recorded.

Multiphoton (three-photon) writing was conducted with the same laser source used for the SHG imaging previously described, while a scanning microscope (Thorlabs, MM101 Multiphoton Microscope) was utilized. A 20x/0.5NA objective (Nikon, CFI Plan Fluor 20X CH) focuses the laser beam as well as collects light above the sample (reflected light microscopy). Afterward, the SHG signal is selected with a SHG filter (Bandpass, 515 nm) in order to perform SHG imaging. During the writing, the total energy output from the laser source was fixed at 300 mW, with a pixel dwell time of 2.5 µs; different irradiation times were given to different scanning areas to keep the same energy loaded for each unit area, such as 1 min for 8 microns square, 4 min for 16 microns square and 16 min for 32 microns square.

The excitation anisotropy measurements were performed using a FluoroMax-4 spectrofluorometer. The experiment was carried out in a viscous medium such as triacetin (η 20 °C = 20 mPa.s). Two Glan-Thompson polarizers are placed in the excitation and emission beams. The anisotropy r is determined as follows:

$$r = \frac{I_{VV} - g I_{VH}}{I_{VV} + 2.g.I_{VH}} \text{ with } g = \frac{I_{HV}}{I_{HH}} \quad (2)$$

where *I* is the fluorescence intensity. The subscripts denote the orientation (horizontal *H* or vertical *V*) of the excitation and emission polarizers, respectively. *g* is an instrumental correction factor. The proper calibration of the set-up was checked using a recent standard method with rhodamine 101 in glycerol.

The theoretical calculations have been computed based on Density Functional Theory (DFT). The overall computation strategy was defined as follows: After initial AM1 optimization calculations, subsequent optimization of the geometrical structure was carried out using the MPW1PW91/6-31G level of calculation. The geometry was then frequently checked. The TDDFT vertical transitions are finally computed using the same level of calculations. All calculations have been performed using the GAUSSIAN 09 package.[30] Note that solvent effects were also included by using the polarizable continuum model (PCM) implemented in Gaussian09 for THF. The molecular orbitals involved in these transitions could be extracted.

Supporting Information

Supporting Information is available from the Wiley Online Library or from the author.

Acknowledgements

This research has been supported by the French National Research Agency (ANR), in the framework of the 3D-ODS research program (Project-ANR-20-CE24-0028) and by the "Région Bretagne" in the framework of the 3D-STORE research program (Project N°241302–UMR6226). Y.D.C. and G.R. acknowledge the support from the Fund for Scientific Research-Flanders (FWO) (1234222N and 1S92624N respectively).

Conflict of Interest

The authors declare no conflict of interest.

Data Availability Statement

The data that support the findings of this study are available from the corresponding author upon reasonable request.

Keywords

liquid crystal, non-linear optic, optical storage, pyrimidine

Received: August 6, 2024
Revised: September 18, 2024
Published online:

[1] a) F. Gallego-Gómez, F. Del Monte, K. Meerholz, *Nat. Mater.* **2008**, *7*, 490; b) C. J. Carling, J. C. Boyer, N. R. Branda, *J. Am. Chem. Soc.* **2009**, *131*, 10838; c) K. Iliopoulos, O. Krupka, D. Gindre, M. Sallé, *J. Am. Chem. Soc.* **2010**, *132*, 14343; d) D. Gindre, A. Boeglin, A. Fort, L. Mager, K. D. Dorkenoo, *Opt. Express* **2006**, *14*, 9896.
[2] H. A. Al Attar, O. Taqatqa, *J. Opt. A Pure Appl. Opt.* **2003**, *5*, S487.
[3] B. Lohse, R. Vestberg, M. T. Ivanov, S. Hvilsted, R. H. Berg, C. J. Hawker, P. S. Ramanujam, *Chem. Mater.* **2008**, *20*, 6715.
[4] a) A. Khan, A. E. Daugaard, A. Bayles, S. Koga, Y. Miki, K. Sato, J. Enda, S. Hvilsted, G. D. Stucky, C. J. Hawker, *Chem. Commun.* **2009**, 425; b) R. Castagna, F. Vita, D. E. Lucchetta, L. Criante, F. Simoni, *Adv. Mater.* **2009**, *21*, 589.
[5] D. A. Parthenopoulos, P. M. Rentzepis, *Science* **1989**, *245*, 843.
[6] a) M. Irie, *Chem. Rev.* **2000**, *100*, 1685; b) A. Toriumi, J. M. Herrmann, S. Kawata, *Opt. Lett.* **1997**, *22*, 555.
[7] Z. Sekkat, W. Knoll, *J. Opt. Soc. Am. B* **1995**, *12*, 1855.
[8] a) C. C. Corredor, Z. L. Huang, K. D. Belfield, *Adv. Mater.* **2006**, *18*, 2910; b) D. Gindre, A. Boeglin, A. Fort, K. D. Mager, L. Dorkenoo, *Opt. Express* **2006**, *14*, 9896.
[9] D. Gindre, K. Iliopoulos, O. Krupka, M. Evrard, E. Champigny, M. Sallé, *Molecules* **2016**, *21*, 147.
[10] B. Lohse, S. Hvilsted, R. H. Berg, P. S. Ramanujam, *Chem. Mater.* **2006**, *18*, 4808.
[11] H. Meier, D. Cao, *Chem. Soc. Rev.* **2013**, *42*, 143.
[12] M. Tu, H. Reinsch, S. Rodríguez-Hermida, R. Verbeke, T. Stassin, W. Egger, M. Dickmann, B. Dieu, J. Hofkens, I. Vankelecom, N. Stock, R. Ameloot, *Angew. Chem.* **2019**, *131*, 2445.
[13] M. C. Spiridon, K. Iliopoulos, F. A. Jerca, V. V. Jerca, D. M. Vuluga, D. S. Vasilescu, D. Gindre, B. Sahraoui, *Dyes Pigm.* **2015**, *114*, 24.
[14] D. Gindre, K. Iliopoulos, O. Krupka, E. Champigny, Y. Morille, M. Sallé, *Opt. Lett.* **2013**, *38*, 4636.
[15] a) D. S. Chemla, J. Zyss, *Nonlinear Optical Properties of Organic Molecules and Crystals*, Academic Press, Orlando, FL (USA) **1987**; b) Z. Zekkat, W. Knoll, *Photoreactive Organic Thin Films*, Academic Press, Elsevier, New York, USA **2002**.
[16] S. van Cleuvenbergen, P. Kędziora, J. L. Fillaut, T. Verbiest, K. Clays, H. Akdas-Kilig, F. Camerel, *Angew. Chem., Int. Ed.* **2017**, *56*, 9546.
[17] P. Nicolas, S. Abdallah, A. Dok, Y. de Coene, O. Jeannin, N. Bellec, J.-P. Malval, T. Verbiest, K. Clays, S. Van Cleuvenbergen, B. Bilgin-Eran, H. Akdas-Kiliç, F. Camerel, *Chem. Asian J.* **2024**, *19*, 202400112.
[18] H. Akdas-Kilig, M. Godfroy, J. L. Fillaut, B. Donnio, B. Heinrich, P. Kędziora, J.-P. Malval, A. Spangenberg, S. Van Cleuvenbergen, K. Clays, F. Camerel, *J. Phys. Chem. C* **2015**, *119*, 3697.
[19] W. Zhai, B. M. Chapin, A. Yoshizawa, H. C. Wang, S. A. Hodge, T. D. James, E. V. Anslyn, J. S. Fossey, *Org. Chem. Front.* **2016**, *3*, 918.
[20] F. Camerel, G. Ulrich, P. Retailleau, R. Ziessel, *Angew. Chem., Int. Ed.* **2008**, *47*, 8876.
[21] M. B. Ros, J. L. Serrano, M. R. De La Fuente, C. L. Folcia, *J. Mater. Chem.* **2005**, *15*, 5093.
[22] a) S. Achelle, J.-P. Malval, S. Aloïse, A. Barsella, A. Spangenberg, L. Mager, H. Akdas-Kilig, J. L. Fillaut, B. Caro, F. Robin-Le Guen, *Chem. Phys. Chem.* **2013**, *14*, 2725; b) J.-P. Malval, S. Achelle, L. Bodiou, A. Spangenberg, L. C. Gomez, O. Soppera, F. Robin-Le Guen, *J. Mater. Chem. C* **2014**, *2*, 7869; c) F. Kournoutas, A. Fihey, J.-P. Malval, A. Spangenberg, M. Fecková, P. L. Poul, C. Katan, F. Robin-Le Guen, F. Bures, S. Achelle, M. Fakis, *Phys. Chem. Chem. Phys.* **2020**, *22*, 4165.
[23] X. Yu, D. Scheller, O. Rademacher, T. Wolff, *J. Org. Chem.* **2003**, *68*, 7386.
[24] C. Xu, W. Denk, W. W. Webb, J. Guild, *Opt. Lett.* **1995**, *20*, 2372.
[25] M. A. Albota, C. Xu, W. W. Webb, *Appl. Opt.* **1998**, *37*, 7352.
[26] N. S. Makarov, M. Drobizhev, A. Rebane, B. H. Cumpston, S. P. Ananthavel, S. Barlow, D. L. Dyer, J. E. Ehrlich, L. L. Erskine, A. A. Heikal, S. M. Kuebler, I.-Y. S. Lee, D. Mccord-Maughon, J. Qin, H. Rockel, M. Rumi, X.-L. Wu, S. R. Marder, J. W. Perry, A. Karotki, M. Kruk, M. Drobizhev, A. Rebane, E. Nickel, C. W. Spangler, *Opt. Express* **2008**, *16*, 4029.
[27] S. de Reguardati, J. Pahapill, M. Rammo, A. Rebane, *Opt. Express* **2016**, *24*, 9053.
[28] S. R. Meech, D. Phillips, *J. Photochem.* **1983**, *23*, 193.
[29] D. V. O' Connor, D. Phillips, *Time-Correlated Single Photon Counting*, Academic Press, London-New York **1984**.
[30] M. J. Frisch, *Gaussian 09, Revision B.01*, Gaussian, Inc, Wallingford CT, **2009**.